Theor Chem Acc (2007) 117:171–181
DOI 10.1007/s00214-006-0170-9

REGULAR ARTICLE

Effective tailor-made force field parameterization of the several Zn coordination environments in the puzzling FTase enzyme: opening the door to the full understanding of its elusive catalytic mechanism

Sérgio Filipe Sousa · Pedro Alexandrino Fernandes · Maria João Ramos

Received: 2 March 2006 / Accepted: 12 April 2006 / Published online: 6 October 2006

Abstract Protein farnesyltransferase (FTase) is very promising anticancer drug target, with several drugs in advanced stages of clinical testing. However, in spite of the thrilling achievements in the development of farnesyltransferase inhibitors (FTIs) over the past few years, the farnesylation mechanism remains, to some degree, a mystery. This work reports the determination and validation of three sets of molecular mechanical parameters specifically tailored to accurately account for the very specific nature of the several Zn coordination spheres formed during the unclear catalytic pathway of this puzzling metalloenzyme, and built on the top of recent experimental and theoretical results that have dramatically changed the way how the farnesylation mechanism is perceived. Extensive validation studies with 14 FTase crystallographic structures, EXAFS data, DFT, and QM/MM theoretical calculations are presented.

Keywords Farnesyltransferase · Zinc enzymes · Force field · Molecular mechanics · Amber

1 Introduction

Protein farnesyltransferase (FTase) is a heterodimeric zinc metalloenzyme, consisting of a 48 kDa α-subunit and a 46 kDa β-subunit [1–4], that has been the subject of great interest in anticancer research over the last decade [5–10]. FTase catalyses the addition of isoprenoid farnesyl from farnesyl diphosphate (FPP), to a cysteine residue of a protein substrate containing a typical –CAAX motif at the carboxyl terminus. In this characteristic motif the C represents the cysteine residue that is farnesylated, A is an aliphatic amino acid, whereas X stands for the terminal amino acid residue, usually methionine, serine, alanine or glutamine [11]. Among the known substrates for FTase are H-, N-, and K-Ras proteins, nuclear lamins A and B, the γ subunit of heterotrimeric G-proteins, and several proteins involved in visual signal transduction [12–14].

Interest in FTase was prompted by the finding that farnesylation is absolutely required for oncogenic forms of Ras proteins to transform cells [15,17], as mutant Ras proteins are responsible for about 30% of all human cancers [18,19]. Examples include pancreatic adenocarcinomas (90%), colon adenocarcinomas and adenomas (50%), lung adenocarcinomas (30%), myeloid leukemias (30%), and melanomas (20%) [20–25]. More than 100 patents describing FTIs have been published since the year 2000 [7], with several drugs in clinical testing [8–10,26–30]. In particular, tipifarnib (Zarnestra; Janssen Pharmaceutica NV) and lonafarnib (Sarasar; Schering-Plough Research Institute) have already been evaluated in phase III clinical trials [31,32]. Nowadays, the development of FTIs as alternative drugs in the treatment of some diseases caused by pathogens, in particular malaria [33,38], Chagas disease [39,41], African sleeping sickness [42–44], Toxoplasmosis [45] and Leishmaniasis [39], and as antiviral agents [46] is also a hot topic of research.

Despite the enormous curiosity surrounding FTase inhibition and the vast research in the field, several

Electronic supplementary material Supplementary material is available in the online version of this article at http://dx.doi.org/10.1007/s00214-006-0170-9 and is accessible for authorized users.

S. F. Sousa · P. A. Fernandes · M. J. Ramos (✉)
REQUIMTE, Departamento de Química,
Faculdade de Ciências, Universidade do Porto,
Rua do Campo Alegre, 687, 4169-007 Porto, Portugal
e-mail: mjramos@fc.up.pt

fundamental features of the farnesylation and inhibition mechanisms remain elusive [47]. The key catalytic role played by the active-site Zn complex has been hindering a successful application of molecular mechanical methods in FTase research, since the well-established biomolecular force fields such as CHARMM [48,49], AMBER [50,51], and GROMOS [52], do not have parameters capable of an accurate treatment of the several different active-site Zn coordination spheres formed. The development of such parameters is a large step in FTase research as it will enable the computer-aided molecular modeling of more specific inhibitors, rationally designed, with increased activity and potential value in the treatment of cancer, malaria, sleeping sickness, or even with application as antiviral agents. Furthermore, it will also promote further insight into the still unsolved catalytic mechanism of this puzzling enzyme [47], particularly when in combination with QM/MM methodologies such as ONIOM [53,54], and the study of the dynamic properties of FTase and of the complexes resultant from its association with the several different inhibitors available.

More than 30 crystallographic structures for FTase have been published since 1997. These X-ray structures refer to several different states of the catalytic and inhibition pathways of this enzyme, and to different combinations of substrates, non-substrates and inhibitors. Despite the high number of crystallographic structures already published doubts remain on the very nature of the active-site Zn coordination sphere [47]. Only recently EXAFS [55] results and some high-level theoretical studies [56,57] have shed some light on this matter, by demonstrating the existence of a carboxylate-shift mechanism, coherent with previous mutagenesis experiments [58], involving Zn ligand Asp297β, both with ligand entrance (bidentate to monodentate) and with product exit (monodentate to bidentate), while showing that during the entire catalytic pathway Zn remains four-coordinated. DFT (B3LYP) calculations, crystallographic data [59–61], and extended X-ray absorption fine structure (EXAFS) results [55] were thoughtfully used in the parameterization, together with new important mechanistic facts obtained from several recent studies [56–65], allowing the development of an effective parameterization scheme specifically tailored for the active site of this enzyme.

This works reports the determination and validation of three sets of parameters, committed to the AMBER force field [50,51], specifically designed to allow a reliable treatment of the puzzling enzyme farnesyltransferase by the use of molecular mechanical methodologies for the three different Zn coordination environments formed during catalysis, comprising a total of four possible targets for the development of FTase inhibitors – FTase resting state, binary complex (FTase–FPP), ternary complex (FTase–FPP–Peptide), and product complex (FTase–Product) – thereby covering the complete mechanistic pathway of this mysterious enzyme.

2 Methodology

2.1 Parameter development

2.1.1 Atom types

The new parameters are intended to be an extension to the AMBER force field [50,51]. For this reason, atom types in conformity with this force field have been adopted. In order to account for the specificity of the three different Zn coordination spheres, in terms of bond lengths, angles and charges, a total of 15 new atom types were also introduced for Zn and the directly coordinated atoms in the three different environments. Figure 1 illustrates the Zn complexes considered and the nomenclature used. Set 1 represents the active-site Zn coordination sphere of the enzyme resting state and binary complex (FTase–FPP). Set 2 represents the Zn complex in the ternary complex (FTase–FPP–Peptide substrate), and Set 3 corresponds to the product complex (FTase–Farnesylated product).

2.1.2 Bond and angle parameters

Given the influence of the nature and identity of the ligands of the Zn coordination sphere on the bond-lengths and angles involving the metal atom, all the bonds containing Zn, and all the angles where Zn was the central atom were computationally parameterized for each of the three models. The angles where Zn was a terminal atom were considered independent of the environment and hence transferable, and were obtained from other Zn enzymes in the literature [66,67].

Initial models for the parameterization process were built from the crystallographic structures with the best resolution for each state – 1FT1 (Set 1), 1JCR (Set 2), and 1 KZP (Set 3) [59–61]. Calculations were performed on the active-site models depicted in Fig. 1, used for the three different sets of parameters. Conventional modeling of the amino acid side chains was used, that is, the zinc ligands aspartate, cysteinate, and histidine were modeled by acetate, methylthiolate, and methylimidazole, respectively. The zinc-bound farnesylated product from Set 3 was modeled by the use of a methylthiolate bonded to the first isoprenoid subunit of FPP. The

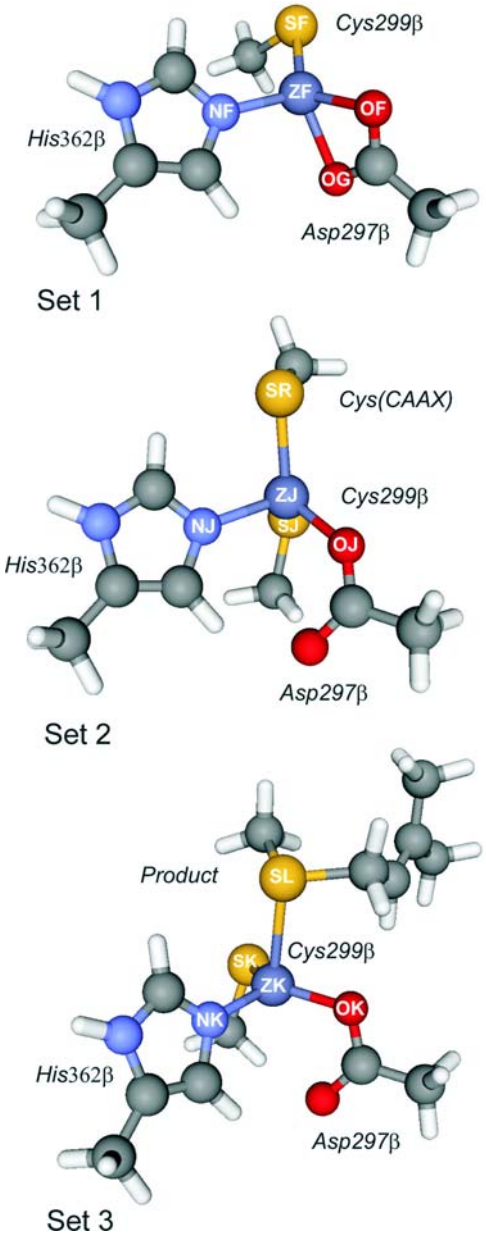

Fig. 1 Zn model complexes considered and nomenclature used in the parameterization process of the three coordination spheres formed during the FTase catalytic pathway. *Set 1* represents the active-site Zn coordination sphere of the enzyme resting state and binary complex (FTase–FPP). *Set 2* illustrates the Zn coordination sphere in the binary complex (FTase–FPP–Peptide), and *Set 3* shows the Zn coordination sphere in the product complex (FTase–Product)

validity of this type of approaches has been demonstrated before with success in the mechanistic study of FTase [56,57], and of several other different enzymes [67–75].

In the parameterization process the density functional theory (DFT) with the B3LYP functional [76,77] was used. DFT calculations have been shown to give very accurate results for systems involving transition metals [78], particularly when using the B3LYP functional [79–81]. For Zn complexes, the superior accuracy of the B3LYP functional in comparison with Hartree–Fock and second-order Moller–Plesset perturbation theory has also been previously demonstrated [69]. Energy minimizations of the models for Sets 1, 2, and 3 were carried out using the SDD basis set, as implemented in Gaussian 03 [82]. This basis set uses the small core quasi-relativistic Stoll–Preuss (SP) electron core potentials (also known as Stuttgart–Dresden) [83,84] for transition elements. For Zn, the outer electrons are described by a (311111/22111/411) valence basis specifically optimized for this metal and for use with the SP pseudopotentials. C, N, and O atoms are accounted by a (6111/41) quality basis set, whereas S and H atoms are treated, respectively, by a (531111/4211) and a (31) quality basis sets. The high-performance of SP pseudopotentials in calculations involving transition metal compounds, particularly within closed-shell systems, has been previously demonstrated [85]. This basis set has also been used before with success in the characterization of the active-site Zn coordination sphere of FTase [56,57].

For each of the three models a series of semi-rigid scans were performed starting from the fully optimized geometry of the model. These scans were performed by gradually changing one of the parameters (positively and negatively) and re-optimizing the model, while keeping the new parameter value fixed and the remaining residues frozen. For example, for the parameterization of the bond Zn–N(His) in model Set 1, both the aspartate and cysteine residues were kept frozen, whereas the zinc atom and the histidine residue were optimized for several Zn–N values around the equilibrium distance. For the angles where Zn is the central atom the same type of principles were applied. In the parameterization of the (Cys)S–Zn–N(His) angle in model Set 1, for example, the aspartate residue was kept frozen, while the Zn atom, the cysteine and histidine residues were optimized for several S–Zn–N values around the equilibrium angle. The resulting potential energy curves were fitted by a least squares method, as exemplified in Fig. 2, for the Zn–N(His) bond and the (Cys)S–Zn–N(His) angle in model Set 1. The force constants for the bonds (K_r) and angles (K_θ) discussed were calculated by considering the following Amber force field expressions for the bonding and angular terms (E_{bond} and E_{angles}):

$$E_{\text{tot}} = \sum_{\text{system}} \left(E_{\text{bond}} + E_{\text{angles}} + E_{\text{torsion}} + E_{\text{VDW}} + E_{\text{electrostatic}}\right) \quad (1)$$

$$E_{\text{bond}} = \sum_{\text{bonds}} K_r (r - r_0)^2 \quad (2)$$

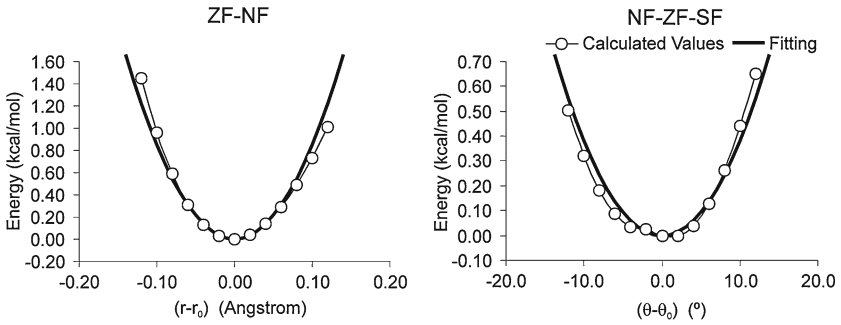

Fig. 2 Parameterization examples for bond ZF–NF and angle NF–ZF–SF, from Eqs. (2) and (3). Energy values calculated at the B3LYP/SDD level from the models depicted in Fig. 1

$$E_{\text{angles}} = \sum_{\text{angles}} K_\theta(\theta - \theta_0)^2. \quad (3)$$

The process was repeated for 4 bonds and 6 angles for each of the 3 models, representing a total of 30 parameters. The equilibrium values of the bond-lengths and angles were determined from the optimizations performed with the models presented in Fig. 1. However, the bond-lengths and angles obtained in other studies with larger models (that included not only the first coordination sphere but also other residues in an 8 Å radius around the zinc atom, ranging from a total of 120–133 atoms) treated following an ONIOM methodology [53,54] at the B3LYP/SDD//PM3 level were also taken into account [56,57]. All quantum mechanical calculations were performed using the Gaussian 03 suite of programs [82].

2.1.3 Dihedral parameters

All the dihedral parameters involving the Zn–ligand interactions were set to zero. This approximation rather simplifies the computational treatment of the system, and confers a certain degree of flexibility to the active-site, without compromising the accurate description of the first coordination sphere of the metal. This procedure has been used with success in the treatment of several different enzymes that have a metal atom covalently bonded [86–91], and is normally viewed as a standard approximation when the bonded model is used with this type of systems [92,93].

2.1.4 van der Waals (VDW) parameters

The VDW parameters for the Zn atom in the three environments considered were taken from a set of studies with the enzyme alcohol dehydrogenase where a bonded potential was also used [67,94,95] , as VDW parameters are commonly taken as transferable between roughly similar environments. Accordingly, for the atoms directly coordinating to the Zn ion VDW parameters were assigned from the closest existing AMBER atom types in the standard AMBER force fields [50,51].

2.1.5 Electrostatic parameters

Restrained ElectroStatic Potential (RESP) charges [96, 97] for the three Zn coordination spheres were derived at the B3LYP/6–311++G(3df,2pd) level. Although the standard AMBER force fields [50,51] were parameterized with HF/6–31G*, in systems involving metals B3LYP is considered a far better method to calculate RESP charges [88], and is commonly used [88,98–101], as HF/6–31G* generally underestimates much of the charge transfer effect involving the metal atom [88,99].

In this process, the models used included the α carbons in addition to the atoms already considered in the models described in Fig. 1, in analogy with the parameterization performed in the FF94, FF96, FF98, and FF99 force fields [50]. The models were energy-minimized with B3LYP/SDD as performed for the first set of models and were build from the same crystallographic structures. The partial charges for the C_α linking atoms were obtained from the correspondent amino acids in the FF99 force field and fixed during the RESP fit procedure, admitting that no significant charge alterations due to the metal–ligand interactions take place beyond the C_α.

2.1.6 Parameterization of the FPP substrate and the farnesylated peptide product

For the FPP molecule, all atom types were defined in conformity with the Amber force field, and no new atom types were introduced (Fig. 3). Bond, Angle, Dihedral, and VDW parameters from the general amber force field (GAFF) were used. Exceptions were the CT–CM–CT and CM–CM–CM angles. For these two angles, force constants were estimated by analogy with angles involving similar atoms in the GAFF, whereas equilibrium angle values were taken directly from the

FPP conformation in the 1JCR X-ray structure [59], the FTase crystallographic structure with an FPP molecule with the best resolution in the PDB. RESP charges were derived using HF/6–31G* in analogy with the GAFF, as this molecule is not involved in ligand–metal charge transfer processes.

In the parameterization of the farnesylated product, a new atom type (SL) was defined (Fig. 3), weakly coordinating the product molecule to the Zn atom, as previously described for the Set 3 model. Parameters for the CM–CT–SL and CT–SL–CT angles were introduced, with force constant defined as described for the FPP molecule, and with equilibrium angle values taken from the 1KZP structure [60] (in the case of CM–CT–SL angle) and from those determined for the Set 3 model (ST–CL–ST angle). The dihedrals involving Zn were set to zero, as performed for parameter Sets 1, 2, and 3. All other bond, angle, dihedral and VDW parameters were taken directly from the GAFF, as performed in the case of FPP. In terms of the electrostatics, the existence of a Zn–SL bond prompts the need to employ B3LYP in the charge determination process. However, in terms of coherence with the remaining parameterization, in particular of the FPP molecule, the farnesylation product should ideally be described by HF/6–31G*. Hence, a combined parameterization protocol was designed. The full farnesylated product was added to model Set 3, and the entire system was subjected to single point energy calculations at both HF/6–31G* and B3LYP/6–311++G(3df,2pd) levels. The charge values obtained from the HF/6–31G* calculation with the RESP procedure for the isoprenoid part of the farnesylated product, were later fixed using RESP to compute charges from the B3LYP/6–311++G(3df,2pd) calculation for the remaining of the model, including the cysteine of the peptidic part of the farnesylated product.

2.2 Parameters validation: molecular dynamics simulations

The three sets of parameters developed were applied to the four key states of the FTase catalytic pathway: FTase resting state, binary complex (FTase–FPP), ternary complex (FTase–FPP–Peptide), and product complex (FTase–Product). The FTase resting state and binary complex share the same Zn coordination sphere with a bidentate aspartate residue [55,56,58], as parameterized for Set 1. For the FTase ternary complex several pieces of evidence have indicated that the peptidic cysteine coordinates Zn as a thiolate and that Asp297β is monodentate [55,56,102], in agreement with the parameters described in Set 2. For the product complex, the existence of direct Zn-product coordination has been

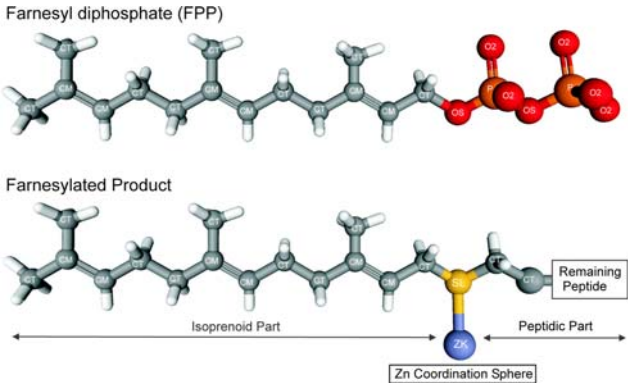

Fig. 3 Schematic representation of the farnesyl diphosphate substrate (FPP) and farnesylated product zinc coordinated with the notation used in the parameterization process

suggested from the available crystallographic structures [60,103], but failed to be confirmed in EXAFS studies [55]. This finding was interpreted as indicative of the existence of a weak Zn–product bond, undetectable by EXAFS. This hypothesis was later confirmed by High-level theoretical calculations and was taken into account in the design of the parameters for Set 3.

The enzyme structures for the validation process were prepared from the crystallographic structures with the best resolution for each state: 1FT1 (Enzyme resting state) [61]; 1FPP (binary complex FTase–FPP) [104]; 1JCR (ternary complex FTase–FPP–Peptide) [59]; and 1KZP (product complex) [60]. The AMBER 8.0 [105] molecular dynamics package was used in the entire process. Conventional protonation states for all amino acids at pH 7 were considered. All the hydrogens were added, and Na^+ ions were placed using the Leap program to neutralize the highly negative charges (ranging from -20 to -24) of the systems. The systems were then placed in rectangular boxes containing TIP3P water molecules, with a minimum distance of 15.0 Å of water molecules between the enzyme and the box side. The total number of atoms in each system was 139,531, 113,054, 133,898, and 134,084, respectively for systems 1 to 4.

All systems were subjected to a four-stage refinement protocol using the SANDER module of AMBER 8.0, in which the constraints on the enzyme were gradually removed. In the first stage (10,000 steps), 50 kcal mol^{-1} Å^{-2} harmonic forces were used to restrain the positions of all atoms in the systems except the ones from the water molecules. In the second stage (10,000 steps) these constraints were applied only to the heavy atoms, and in the third stage (30,000 steps) were limited to the CA and N atom-type atoms (backbone alpha carbons and nitrogens). This process ended in a full energy minimization (fourth stage, maximum 80,000 steps) until the rms gradient was smaller than 0.02 kcal mol^{-1}.

MD simulations on the four systems were carried out using the SANDER module of AMBER 8.0, and considering periodic boundary conditions to simulate a continuous system. The SHAKE algoritm [106] was applied to fix all bond lengths involving a hydrogen bond, permitting a 2 fs time step. The Particle-Mesh Ewald (PME) method [107] was used to include the long-range interactions, and a non-bond-interaction cut-off radius of 10 Å was considered. Following a 50 ps equilibration procedure, 500 ps MD simulations were carried out at 300 K, using Berendsen temperature coupling [108] and constant pressure (1 atm) with isotropic molecule-based scaling. This simulation time is large enough to adequately sample the structural variables that have been parameterized, as bond lengths and angles possess a fast dynamics and no slow conformational rearrangements are possible to occur in the parameterized region (neither are expected, based on the available experimental structural data). Frequency calculations on the models presented in Fig. 1 at the B3LYP/SDD level, have rendered values for the bonds and angles parameterized in this study ranging from 400 cm^{-1} to around 30 cm^{-1}, implying frequency periods of between 0.1 ps (for bonds) and 1 ps (for the angles). Hence, each Zn parameter is sampled at least 500 times during the overall MD simulation, with each bond typically sampled around 5,000 times. The MD trajectory was sampled every 0.2 ps. All of the MD results were analyzed with the PTRAJ module of AMBER8.0, with major emphasis being given to the Zn coordination sphere in the four systems studied.

3 Results and discussion

3.1 Parameter determination

The bonding and angle parameters determined for the three zinc coordination environments are presented in Table 1. A total of 12 bonds and 18 angles were parameterized. Starting from the equilibrium geometries 60 scans were performed (2 for each parameter). Table 2 lists the RESP atomic charges calculated for the key atoms in the Zn active-site. RESP atomic charges for the remaining atoms in the three sets considered, and for the FPP and farnesylated product molecules are presented in the supporting information.

3.2 Validation studies

The parameters derived for the different Zn environments formed during farnesylation were tested in MD simulations of the four key states of the FTase catalytic mechanism: FTase resting state, binary complex (FTase–FPP), ternary complex (FTase–FPP–Peptide) and product complex (FTase–Product). Table 3 lists the average values from the MD simulations performed for the bonds and angles parameterized, considering the instantaneous values collected at every 0.2 ps (after the initial 100 ps). Figure 4 represents the variation in time of the bonds and angles parameterized in the four states considered.

Table 1 Bonding and angle parameters for protein farnesyltransferase (FTase)

Set 1 – FTase resting state and binary complex		
Bonds	K_r (kcal mol^{-1} $Å^{-2}$)	R_{eq} (Å)
ZF–OF	62.3	2.094
ZF–OG	43.8	2.159
ZF–NF	88.3	2.043
ZF–SF	115.8	2.258
Angles	K_θ (kcal mol^{-1} rad^{-2})	θ_{eq} (degrees)
OF–ZF–OG	318.9	63.5
OF–ZF–NF	16.7	107.3
OF–ZF–SF	16.5	126.6
OG–ZF–NF	19.4	97.0
OG–ZF–SF	15.4	136.9
NF–ZF–SF	16.2	114.5
Set 2 – FTase ternary complex		
Bonds	K_r (kcal mol^{-1} $Å^{-2}$)	R_{eq} (Å)
ZJ–OJ	88.3	1.999
ZJ–SJ	81.2	2.352
ZJ–NJ	62.6	2.129
ZJ–SR	69.3	2.373
Angles	K_θ (kcal mol^{-1} rad^{-2})	θ_{eq} (degrees)
OJ–ZJ–NJ	27.8	100.2
OJ–ZJ–SJ	23.0	114.0
OJ–ZJ–SR	24.1	115.1
SJ–ZJ–NJ	20.7	110.1
SJ–ZJ–SR	27.3	116.0
NJ–ZJ–SR	39.1	98.8
Set 3 – FTase product complex		
Bonds	K_r (kcal mol^{-1} $Å^{-2}$)	R_{eq} (Å)
ZK–OK	85.3	1.977
ZK–SK	108.3	2.280
ZK–NK	84.8	2.055
ZK–SL	26.6	2.660
Angles	K_θ (kcal mol^{-1} rad^{-2})	θ_{eq} (degrees)
OK–ZK–NK	18.8	108.2
OK–ZK–SK	15.2	127.6
OK–ZK–SL	24.6	92.3
SK–ZK–NK	12.6	118.7
SK–ZK–SL	16.8	101.6
NK–ZK–SL	22.1	99.1

Table 2 RESP Charges for the key atoms in the active-site of FTase

Atom type	Charge
Set 1 – FTase resting state and binary complex	
ZF	0.9091
OF	−0 .6476
OG	−0 .9126
NF	−0 .3587
SF	−0 .6025
Set 2 – FTase ternary complex	
ZJ	0.8019
OJ	−0 .6620
SJ	−0 .6497
NJ	−0 .0218
SR	−0 .6671
Set 3 – FTase product complex	
ZK	0.4213
OK	−0 .4757
SK	−0 .5959
NK	−0 .0102
SL	−0 .3269

Table 4 presents the average root-mean-square deviation (RMSd) for the backbone C_α atoms (CA) and for the zinc coordination sphere atoms (Zn Core). The Zn Core was defined in analogy with the models described in Fig. 1. Figure 5 illustrates the CA and Zn Core RMSd variation with time in the four states considered. From Table 4 and Figs. 4 and 5 it is obvious that the geometry of the three Zn coordination spheres was maintained very well for the entire simulation time.

To check the validity of the parameters developed, a full-scale comparison of the average Zn bond-lengths obtained from the MD simulations, with EXAFS data [55], a total of 14 X-ray crystallographic structures, and quantum chemical results with small (up to 44 atoms at the B3LYP/SDD level) and larger models (ranging 120–133 atoms at the B3LYP/SDD:PM3 level) [56,57] was performed. The results are summarized in Fig. 6, with major emphasis being given to the EXAFS data,

Table 4 Root-mean-square deviation (RMSd) summary of the simulations performed (after the initial 100 ps)

RMSd (Å)	Resting state	Binary complex	Ternary complex	Product complex
CA	1.4 ± 0.2	1.2 ± 0.1	1.1 ± 0.1	1.3 ± 0.2
Zinc core	0.27 ± 0.05	0.39 ± 0.07	0.74 ± 0.09	0.22 ± 0.06

the most precise data available, as the existing X-ray structures have almost all resolutions poorer than 2 Å . From Fig. 6 the excellent agreement between the MD results with the newly developed parameters and the experimental and quantum chemical results is evident. The agreement with experimental data is remarkable, in particular taking into consideration that the values for the bonds-lengths and angles parameterized were taken from the small quantum chemical active-site models. In fact, the MD simulations performed yielded results than are in most of the cases better than the X-ray results themselves, and are in closer agreement with the EXAFS data and the higher-quality X-ray structures.

A very simple earlier attempt to analyze FTase using MD, employed the ingenious cationic dummy atom approach [109]. This method does not take into account covalent bonds or harmonic constraints at the Zn complex. Instead, the Zn atom is substituted by four cationic dummy atoms tetrahedrically placed around the Zn nucleus, imposing a tetrahedral coordination geometry to the complex. Success was naturally limited by the drastic approaches considered [109–112]. The method requires ligands in the first coordination sphere to be deprotonated to negatively charged species not to lose contact with the dummy atoms introduced. In addition to this, the negatively charged second-sphere ligands normally have to be protonated as to avoid attack at the charged dummy atoms.

The present full set of FTase tailor-made MD parameters here introduced allow an effective modeling of

Table 3 Average values and standard deviations for the parameterized bond-lengths and angles calculated from the MD runs after the first 100 ps

Resting state		Binary complex		Ternary complex		Product complex	
Average bonds-lengths ± deviation (Å)							
ZF–OF	2.06 ± 0.06	ZF–OF	2.09 ± 0.06	ZJ–OJ	1.95 ± 0.06	ZK–OK	1.95 ± 0.06
ZF–OG	2.15 ± 0.07	ZF–OG	2.13 ± 0.07	ZJ–SR	2.44 ± 0.07	ZK–SL	2.6 ± 0.1
ZF–SF	2.23 ± 0.05	ZF–SF	2.24 ± 0.05	ZJ–SJ	2.36 ± 0.06	ZK–SK	2.28 ± 0.06
ZF–NF	2.02 ± 0.06	ZF–NF	2.03 ± 0.06	ZJ–NJ	2.19 ± 0.07	ZK–NK	2.08 ± 0.06
Average angles ± deviation (degrees)							
NF–ZF–SF	119 ± 5	NF–ZF–SF	114 ± 6	NJ–ZJ–SR	99 ± 4	OK–ZK–NK	111 ± 6
OF–ZF–NF	101 ± 6	OF–ZF–NF	102 ± 7	OJ–ZJ–NJ	110 ± 5	OK–ZK–SK	118 ± 6
OF–ZF–OG	64 ± 1	OF–ZF–OG	63 ± 1	OJ–ZJ–SJ	113 ± 5	OK–ZK–SL	87 ± 5
OF–ZF–SF	123 ± 6	OF–ZF–SF	124 ± 6	OJ–ZJ–SR	102 ± 7	SK–ZK–NK	125 ± 5
OG–ZF–NF	81 ± 4	OG–ZF–NF	80 ± 5	SJ–ZJ–NJ	118 ± 5	SK–ZK–SL	101 ± 6
SF–ZF–OG	84 ± 6	SF–ZF–OG	83 ± 6	SJ–ZJ–SR	112 ± 5	NK–ZK–SL	103 ± 5

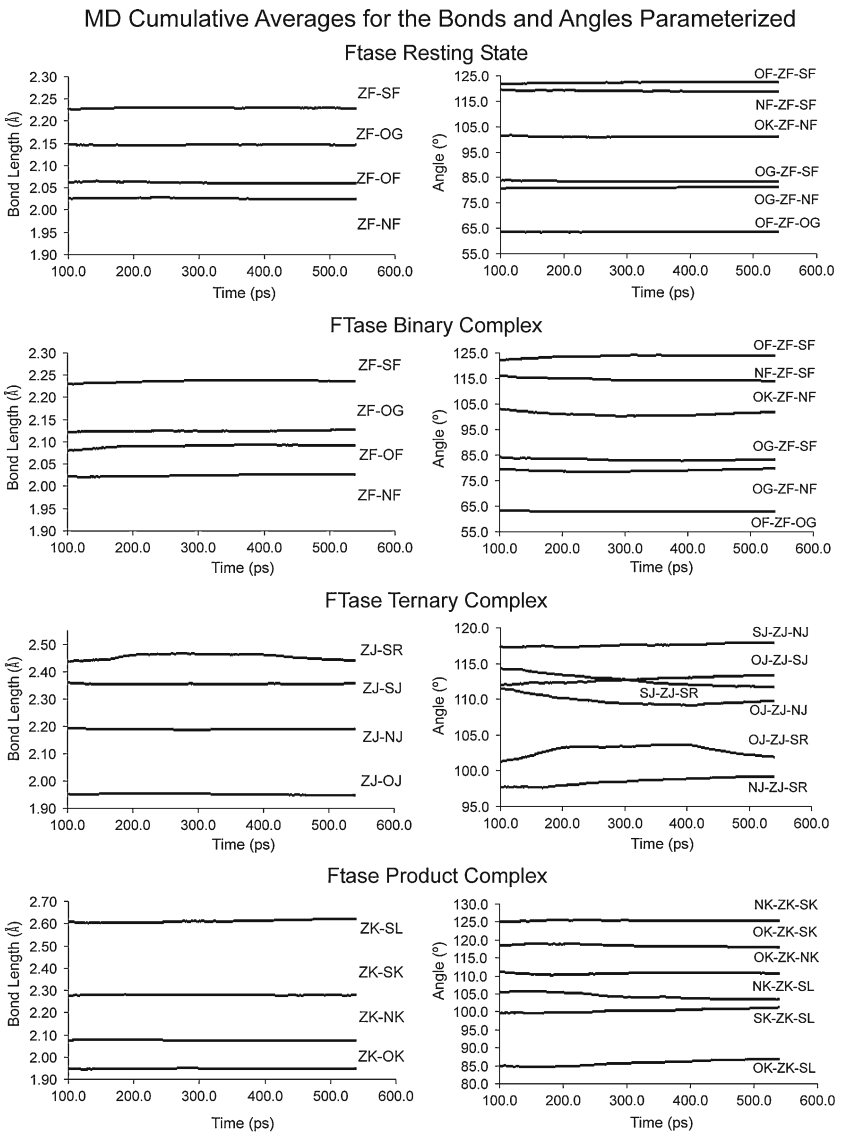

Fig. 4 Plots of the molecular dynamics (MD) cumulative averages for all bonds and angles parameterized for the Zn Coordination Spheres in the FTase resting state, binary complex, ternary complex, and product complex, calculated after the initial 100 ps of simulation

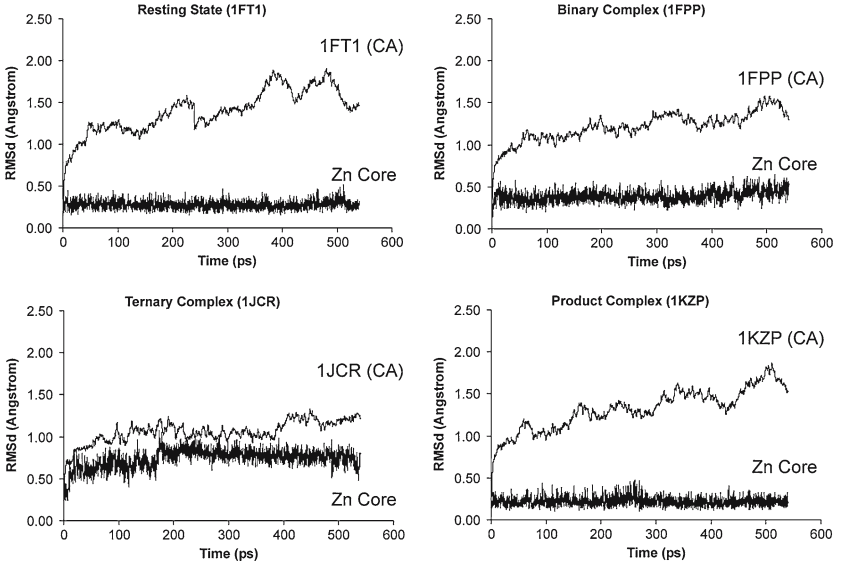

Fig. 5 Graphic representations of the root-mean-square deviation (RMSd) variation in the MD simulations performed for the four systems considered: FTase resting state, binary complex, ternary complex, and product complex. The Zn Core RMSd refers to the RMSd values for the atoms in the Zn respective coordination sphere throughout the simulation protocol

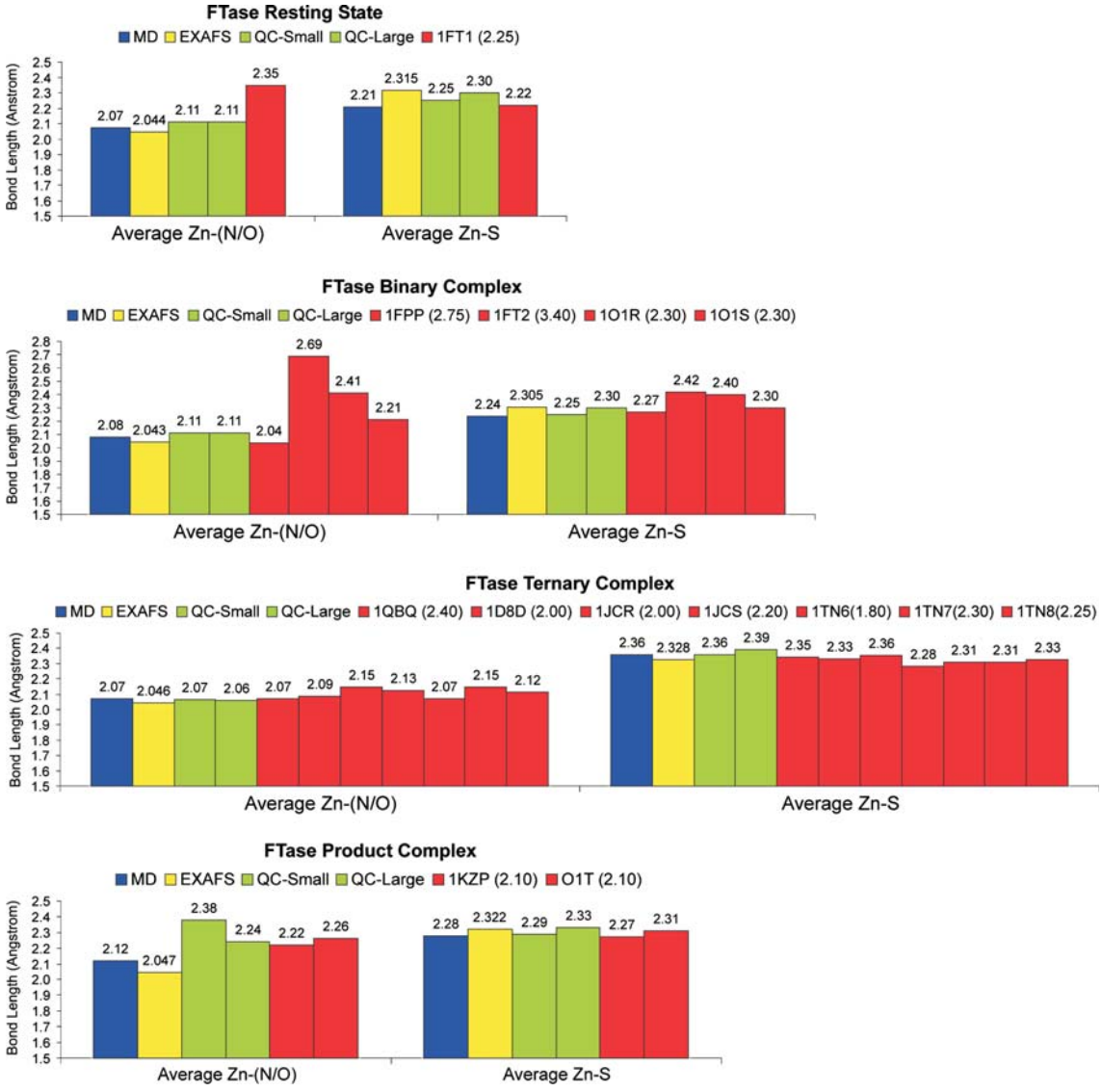

Fig. 6 Parameter validation comparison of results obtained by MD simulation (using the parameters developed) against EXAFS data, quantum calculations with small (up to 44 atoms) and larger (ranging from a total of 120–133 atoms) models (QC Small and QC Large), and 14 X-ray crystallographic structures (PDB code, resolution *indicated in parentheses*)

the four key-states of the FTase catalytic pathway with notable accuracy, in agreement with X-ray and EXAFS experimental evidence, and with the data obtained from high-level quantum studies on small active-site models. Altogether, the parameters derived comprise a powerful tool to an integrated dynamic analysis of the several states formed during the farnesylation mechanism, opening the way to a full understanding of the FTase activity.

4 Concluding remarks

Three sets of parameters specifically designed to account for the several changes that take place at the Zn coordination sphere in the FTase catalytic mechanism have been derived through a combination of theoretical calculations and experimental data, taking into consideration the most recently reported mechanistic facts and the novel views on the FTase catalytic mechanism. These parameters were applied with great success in MD simulations of the four different key states of the FTase catalytic mechanism – FTase resting state, binary complex (FTase–FPP), ternary complex (FTase–FPP–Peptide), and product complex (FTase–Product) – and extensively validated against EXAFS data, a total of 14 X-ray crystallographic structures, and high-level quantum calculations with two types of models of different sizes.

The collection of parameters here presented constitute a global framework that allows the stable and coherent MD study of the several key intermediates formed during the FTase catalytic pathway, and opens the door to a full scale integrated analysis of the several aspects involved in the farnesylation process, and to a deeper understanding of the elusive nature of the FTase catalytic and inhibition pathways.

Acknowledgements We thank the FCT (Fundação para a Ciência e a Tecnologia) for financial support (POCI/QUI/61563/2004). Sérgio Filipe Sousa also acknowledges the FCT for a doctoral scholarship (SFRH/BD/12848/2003).

References

1. Chen WJ, Andres DA, Goldstein JL, Russell DW, Brown MS (1991) Cell 66:327
2. Chen WJ, Andres DA, Goldstein JL, Brown MS (1991) Proc Natl Acad Sci USA 88:11368
3. Reiss Y, Goldstein JL, Seabra MC, Casey PJ, Brown MS (1990) Cell 62:81
4. Reiss Y, Seabra MC, Armstrong SA, Slaughter CA, Goldstein JL, Brown MS (1991) J Biol Chem 266:10672
5. Johnston SR (2001) Lancet Oncol 2:18
6. Sebti SM (2003) Oncologist 8:30
7. Huang CY, Rokosz L (2004) Expert Opin Therap Patents 14:175
8. Adjei AA (2005) Cancer Chemother Biol Response Modif 22:123
9. Appels NMGM, Beijnen JH, Schellens JHM (2005) Oncologist 10:565
10. Kurzrock R (2005) Clin Adv Hematol Oncol 3:161
11. Moores SL, Schaber MD, Mosser SD, Rands E, O'Hara MB, Garsky VM, Marshall MS, Pompliano DL, Gibbs JB (1991) J Biol Chem 266:14603
12. Schafer WR, Rine J (1992) Annu Rev Genet 26:209
13. Glomset JA, Farnsworth CC (1994) Annu Rev Cell Biol 10:181
14. Zhang FL, Casey PJ (1996) Annu Rev Biochem 65:241
15. Hancock JF, Magee AI, Childs JE, Marshall CJ (1989) Cell 57:1167
16. Jackson JH, Cochrane CG, Bourne JR, Solski PA, Buss JE, Der CJ (1990) Proc Natl Acad Sci USA 87:3042
17. Kato K, Cox AD, Hisaka MM, Graham SM, Buss JE, Der CJ (1992) Proc Natl Acad Sci USA 89:6403
18. Dolence JM, Poulter CD (1995) Proc Natl Acad Sci USA 92:5008
19. Takai Y, Sasaki T, Matozaki T (2001) Physiol Rev 81:153
20. Barbacid M (1987) Annu Rev Biochem 56:779
21. Bos JL (1989) Cancer Res 49:4682
22. Almoguera C, Shibata D, Forrester K, Martin J, Arnheim N, Perucho M (1988) Cell 53:549
23. Rodenhuis S, Slebos RJ, Boot AJ, Evers SG, Mooi WJ, Wagenaar SS, Van Bodegom PC, Bos JL (1988) Cancer Res 48:5738
24. Bos JL, Fearon ER, Hamilton SR, Verlaan-de Vries M, Van Boom JH, Van der Eb AJ, Vogelstein B (1987) Nature 327:293
25. Vogelstein B, Fearon ER, Hamilton AD, Kern SE, Preisinger AC, Leppert M, Nakamura Y, White R, Smits AM, Bos JL (1988) New Engl J Med 319:525
26. Ayral-Kaloustian S, Salaski EJ (2002) Curr Med Chem 9:1003
27. Ohkanda J, Knowles DB, Blaskovich MA, Sebti SM, Hamilton AD (2002) Curr Top Med Chem 2:303
28. Brunner TB, Hahn SM, Gupta AK, Muschel RJ, McKenna WG, Bernhard EJ (2003) Cancer Res 63:5656
29. Caponigro F, Casale M, Bryce J (2003) Expert Opin Investig Drugs 12:943
30. Doll RJ, Kirschmeier P, Bishop WR (2004) Curr Opin Drug Discov Dev 7:478
31. Van Cutsem E, van de Velde H, Karasek P, Oettle H, Vervenne WL, Szawlowski A, Schoffski P, Post S, Verslype C, Neumann H, Safran H, Humblet Y, Perez Ruixo J, Ma Y, Von Hoff D (2004) J Clin Oncol 22:1430
32. Rao S, Cunningham D, de Gramont A, Scheithauer W, Smakal M, Humblet Y, Kourteva G, Iveson T, Andre T, Dostalova J, Illes A, Belly R, Perez-Ruixo JJ, Park YC, Palmer PA (2004) J Clin Oncol 22:3950
33. Chakrabarti D, Da Silva T, Barger J, Paquette S, Patel H, Patterson S, Allen CM (2002) J Biol Chem 277:42066
34. Wiesner J, Kettler K, Sakowski J, Ortmann R, Katzin A, Kimura E, Silber K, Klebe G, Jomaa H, Schlitzer M (2004) Angew Chem Int Ed Engl 43:251
35. Kettler K, Wiesner J, Silber K, Haebel P, Ortmann R, Sattler I, Dahse HM, Jomaa H, Klebe G, Schlitzer M (2005) Eur J Med Chem 40:93
36. Eastman RT, White J, Hucke O, Bauer K, Yokoyama K, Nallan L, Chakrabarti D, Verlinde CLMJ, Gelb MH, Rathod PK, Van Voorhis WC (2005) J Biol Chem 280:13554
37. Glenn MP, Chang SY, Hucke O, Verlinde CL, Rivas K, Horney C, Yokoyama K, Buckner FS, Pendyala PR, Chakrabarti D, Gelb M, Van Voorhis WC, Sebti SM, Hamilton AD (2005) Angew Chem Int Ed Engl 44:4903
38. Nallan L, Bauer KD, Bendale P, Rivas K, Yokoyama K, Horney CP, Pendyala PR, Floyd D, Lombardo LJ, Williams DK, Hamilton A, Sebti S, Windsor WT, Weber PC, Buckner FS, Chakrabarti D, Gelb MH, Van Voorhis WC (2005) J Med Chem 48:3704
39. Buckner FS, Eastman RT, Nepomuceno-Silva JL, Speelmon EC, Myler PJ, Van Voorhis WC, Yokoyama K (2002) Mol Biochem Parasitol 122:181
40. Esteva MI, Kettler K, Maidana C, Fichera L, Ruiz AM, Bontempi EJ, Andersson B, Dahse HM, Haebel P, Ortmann R, Klebe G, Schlitzer M (2005) J Med Chem 48:7186
41. Hucke O, Gelb MH, Verlinde CL, Buckner FS (2005) J Med Chem 48:5415
42. Yokoyama K, Trobridge P, Buckner FS, Van Voorhis WC, Stuart KD, Gelb MH (1998) J Biol Chem 273:26497
43. Buckner FS, Yokoyama K, Nguyen L, Grewal A, Erdjument-Bromage H, Tempst P, Strickland CL, Xiao L, Van Voorhis WC, Gelb MH (2000) J Biol Chem 275:21870
44. Ohkanda J, Buckner FS, Lockman JW, Yokoyama K, Carrico D, Eastman R, Luca-Fradley K, Davies W, Croft SL, Van Voorhis WC, Gelb MH, Sebti SM, Hamilton AD (2004) J Med Chem 47:432
45. Ibrahim M, Azzouz N, Gerold P, Schwarz RT (2001) Int J Parasitol 31:1489
46. Bordier BB, Ohkanda J, Liu P, Lee SY, Salazar FH, Marion PL, Ohashi K, Meuse L, Kay MA, Casey JL, Sebti SM, Hamilton AD, Glenn JS (2003) J Clin Invest 112:407
47. Sousa SF, Fernandes PA, Ramos MJ (2005) J Biol Inorg Chem 10:3
48. Brooks BR, Bruccoleri RE, Olafson BD, States DJ, Swaminathan S, Karplus M (1983) J Comput Chem 4:187
49. MacKerell AD, Wiorkiewiczkuczera J, Karplus M (1995) J Am Chem Soc 117:11946

50. Cornell WD, Cieplak P, Bayly CI, Gould IR, Merz KM, Fergunson DM, Spellmeyer DC, Fox T, Caldwell JW, Kollman PA (1995) J Am Chem Soc 117:5179
51. Weiner SJ, Kollman PA, Case DA, Singh UC, Ghio C, Alagona G, Profeta S, Weiner P (1984) J Am Chem Soc 106:765
52. Hermans J, Berendsen HJC, Vangunsteren WF, Postma JPM (1984) Biopolymers 23:1513
53. Dapprich S, Komaromi I, Byun KS, Morokuma K, Frisch MJ (1999) J Mol Struct (Theochem) 461:1
54. Vreven T, Morokuma K (2000) J Comput Chem 21:1419
55. Tobin DA, Pickett JS, Hartman HL, Fierke CA, Penner-Hahn JE (2003) J Am Chem Soc 125:9962
56. Sousa SF, Fernandes PA, Ramos MJ (2005) J Mol Struct (Theochem) 729:125
57. Sousa SF, Fernandes PA, Ramos MJ (2005) Biophys J 88:483
58. Fu HW, Beese LS, Casey PJ (1998) Biochemistry 37:4465
59. Long SB, Hancock PJ, Kral AM, Hellinga HW, Beese LS (2001) Proc Natl Acad Sci USA 98:12948
60. Long SB, Casey PJ, Beese LS (2002) Nature 419:645
61. Park HW, Boduluri SR, Moomaw JF, Casey PJ, Beese LS (1997) Science 275:1800
62. Pickett JS, Bowers KE, Fierke CA (2003) J Biol Chem 278:51243
63. Pickett JS, Bowers KE, Hartman HL, Fu HW, Embry AC, Casey PJ, Fierke CA (2003) Biochemistry 42:9741
64. Bowers KE, Fierke CA (2004) Biochemistry 43:5256
65. Hartman HL, Bowers KE, Fierke CA (2004) J Biol Chem 279:30546
66. Merz KM Jr (1991) J Am Chem Soc 113:406
67. Ryde U (1995) Proteins 21:40
68. Siegbahn PEM (1998) J Am Chem Soc 120:8417
69. Ryde U (1999) Biophys J 77:2777
70. Fernandes PA, Ramos MJ (2003) Chem Eur J 9:5916
71. Fernandes PA, Ramos MJ (2003) J Am Chem Soc 125:6311
72. Lucas MF, Fernandes PA, Eriksson LA, Ramos MJ (2003) J Phys Chem B 107:5751
73. Pereira S, Fernandes PA, Ramos MJ (2004) J Comput Chem 25:1286
74. Pereira S, Fernandes PA, Ramos MJ (2004) J Comput Chem 25:227
75. Pereira S, Fernandes PA, Ramos MJ (2005) J Am Chem Soc 127:5174
76. Becke AD (1993) J Chem Phys 98:5648
77. Lee C, Yang WT, Parr RG (1988) Phys Rev B 37:785
78. Ziegler T (1991) Chem Rev 91:651
79. Bauschlicher CW (1995) Chem Phys Lett 246:40
80. Holthausen MC, Mohr M, Koch W (1995) Chem Phys Lett 240:245
81. Ricca A, Bauschlicher CW (1995) Theor Chim Acta 92:123
82. Frisch MJ, Trucks GW, Schlegel HB, Scuseria GE, Robb MA, Cheeseman JR, Montgomery JA, Vreven T, Kudin KN, Burant JC, Millam JM, Iyengar SS, Tomasi J, Barone V, Mennucci B, Cossi M, Scalmani G, Rega N, Petersson GA, Nakatsuji H, Hada M, Ehara M, Toyota K, Fukuda R, Hasegawa J, Ishida M, Nakajima T, Honda Y, Kitao O, Nakai H, Klene M, Li X, Knox JE, Hratchin HP, Cross JB, Adamo C, Jaramillo J, Gomperts R, Stratmann RE, Yazyev O, Austin AJ, Cammi R, Pomelli C, Ochterski JW, Ayala PY, Morokuma K, Voth GA, Salvador P, Dannenberg JJ, Zakrzewski VG, Dapprich S, Daniels AD, Strain MC, Farkas O, Malik DK, Rabuck AD, Raghavachari K, Foresman JB, Ortiz JV, Cui Q, Baboul AG, Clifford S, Cioslowski J, Stefanov BB, Liu G, Liashenko A, Piskorz P, Komaromi I, Martin RL, Fox DJ, Keith T, Al-Lahan A, Peng CY, Nanayakkara A, Challacombe M, Gill PMW, Johnson B, Chen W, Wong MW, Gonzalez C, Pople JA (2003) Gaussian, Inc, Pittsburg PA,
83. Andrae D, Haussermann U, Dolg M, Stoll H, Preuss H (1990) Theor Chim Acta 77:123
84. Dolg M, Wedig U, Stoll H, Preuss H (1987) J Chem Phys 86:866
85. Frenking G, Antes I, Bohme M, Dapprich S, Ehlers AW, Jonas V, Neubaus A, Otto M, Stegmann R, Veldkamp A, Vyboishchikov SF (1996) Rev Comput Chem 8:63
86. Hoops SC, Anderson KW, Merz KM Jr (1991) J Am Chem Soc 113:8262
87. Merz KM Jr, Banci L (1997) J Am Chem Soc 119:863
88. Yao L, Sklenak S, Yan H, Cukier RI (2005) J Phys Chem B 109:7500
89. Park H, Lee S (2004) J Comput Aided Mol Des 18:375
90. Suarez D, Merz KM Jr (2001) J Am Chem Soc 123:3759
91. Park H, Merz KM Jr (2005) J Med Chem 48:1630
92. Comba P, Remenyi R (2003) Coord Chem Rev 238–239:9
93. Zimmer M (1995) Chem Rev 95:2629
94. Ryde U (1995) Protein Sci 4:1124
95. Ryde U (1996) J Comput Aided Mol Des 10:153
96. Bayly CI, Cieplak P, Cornell WD, Kollman PA (1993) J Phys Chem 97:10269
97. Cieplak P, Cornell WD, Bayly CI, Kollman PA (1995) J Comput Chem 16:1357
98. Banci L (2003) Curr Opin Chem Biol 7:143
99. Suarez D, Brothers EN, Merz KM Jr (2002) Biochemistry 41:6615
100. Lecerof D, Fodje MN, Leon RA, Olsson U, Hansson A, Sigfridsson E, Ryde U, Hansson M, Al-Karadaghi S (2003) J Biol Inorg Chem 8:452
101. Gilboa R, Spungin-Bialik A, Wohlfahrt G, Schomburg D, Blumberg S, Shoham G (2001) Proteins 44:490
102. Hightower KE, Huang CC, Casey PJ, Fierke CA (1998) Biochemistry 37:15555
103. Turek-Etienne TC, Strickland CL, Distefano MD (2003) Biochemistry 42:3716
104. Dunten P, Kammlott U, Crowther R, Weber D, Palermo R, Birktoft J (1998) Biochemistry 37:7907
105. Case DA, Darden TA, Cheatham III TE, Simmerling CL, Wang J, Duke RE, Luo R, Merz KM, Wang B, Pearlman DA, Crowley M, Brozell S, Tsui V, Gohlke H, Mongan J, Hornak V, Cui G, Beroza P, Schafmeister C, Caldwell JW, Ross WS, Kollman PA (2004) University of California, San Francisco
106. Ryckaert JP, Ciccotti G, Berendsen HC (1977) J Comput Phys 23:327
107. Essman V, Perera L, Berkowitz ML, Darden T, Lee H, Pedersen LG (1995) J Chem Phys 103:8577
108. Berendsen HC, Postma JPM, van Gunsteren WF, DiNola A, Haak JR (1984) J Comput Phys 81:3684
109. Pang YP, Xu K, Yazal JE, Prendergas FG (2000) Protein Sci 9:1857
110. Pang YP (1999) J Mol Model 5:196
111. Pang YP (2001) Proteins 45:183
112. Oelschlaeger P, Schmid RD, Pleiss J (2003) Protein Eng 16:341